



Simultaneous adsorption of Cd(II) and phosphate on Al₁₃ pillared montmorillonite

Journal:	<i>RSC Advances</i>
Manuscript ID:	RA-ART-08-2015-015744
Article Type:	Paper
Date Submitted by the Author:	06-Aug-2015
Complete List of Authors:	MA, Lingya; Guangzhou Institute of Geochemistry, Chinese Academy of Sciences, ; Queensland University of Technology, Zhu, Jianxi; Guangzhou Institute of Geochemistry, Chinese Academy of Sciences, Xi, Yunfei; Queensland University of Technology, Zhu, Runliang; Guangzhou Institute of Geochemistry, Chinese Academy of Sciences guangzhou, guangdong, China, He, Hongping; Guangzhou Institute of Geochemistry, Chinese Academy of Sciences, Liang, Xiaoliang; Guangzhou Institute of Geochemistry, Chinese Academy of Sciences, Ayoko, Godwin; Queensland University of Technology, Chemistry, Physics & Mechanic Engineering

Simultaneous adsorption of Cd(II) and phosphate on Al₁₃ pillared montmorillonite

Lingya Ma^{a,b,c}, Jianxi Zhu^{a,d}, Yunfei Xi^{b*}, Runliang Zhu^{a,d}, Hongping He^{a,d*}, Xiaoliang Liang^{a,d}
Godwin A. Ayoko^b

^aKey Laboratory of Mineralogy and Metallogeny, Guangzhou Institute of Geochemistry, Chinese Academy of Sciences, Guangzhou 510640, China

^bNanotechnology and Molecular Science Discipline, Faculty of Science and Engineering, Queensland University of Technology, 2 George Street, GPO Box 2434, Brisbane, QLD 4000, Australia.

^cUniversity of Chinese Academy of Sciences, Beijing 100049, China

^dGuangdong Provincial Key Laboratory of Mineral Physics and Material, Guangzhou 510640, China

*Corresponding authors:

Dr Yunfei Xi

Tel: +61 7 3138 1466

E-mail address: y.xi@qut.edu.au

Prof Hongping He

Tel: +86 020 8529 0257

E-mail address: hehp@gig.ac.cn

Abstract

Al₁₃ pillared montmorillonites (AIPMTs) prepared with different Al/clay ratios were used to remove Cd(II) and phosphate from aqueous solution. The structure of AIPMTs was characterized by X-ray diffraction (XRD), Thermogravimetric analysis (TG), and N₂ adsorption-desorption. The basal spacing, intercalated amount of Al₁₃ cations, and specific surface area of AIPMTs increased with the increase of Al/clay ratio. In the single adsorption system, with the increase of Al/clay ratio, the adsorption of phosphate on AIPMTs increased but that of Cd(II) decreased. Significantly enhanced adsorptions of Cd(II) and phosphate on AIPMTs were observed in a simultaneous system. For both contaminants, the adsorption of one contaminant would increase with the increase of initial concentration of the other one and increase in the Al/clay ratio. The enhancement of adsorption of Cd(II) was much higher than that of phosphate on AIPMT. This suggests that the intercalated Al₁₃ cations are the primary co-adsorption sites for phosphate and Cd(II). X-ray photoelectron spectroscopy (XPS) indicated comparable binding energy of P2p but different binding energy of Cd3d in single and simultaneous systems. The adsorption and XPS results suggested that the formation of P-bridge ternary surface complexes were the possible adsorption mechanism for promoted uptake of Cd(II) and phosphate on AIPMT.

Keywords: Co-adsorption; Al₁₃ pillared montmorillonite; Cadmium; Phosphate; Heavy metals.

1. Introduction

Heavy metal cations (*e.g.* cadmium) and oxyanions (*e.g.* phosphate) are the typical inorganic contaminants in environment. Heavy metals are released from industrial sites and ultimately transported into water and soil, where they may become a potential threat to human health via the food chain.¹ For example, being a carcinogen chemical, Cd(II) is one of extremely toxic heavy metals in soil and wastewater and could accumulate in plants, animals, and human beings.² As an essential nutrient for plants and crops, phosphate with high concentration in water also causes risks to the environment, and an example of its adverse consequence is the accelerated eutrophication in lakes and coastal waterways.^{3, 4} In contrast to organic toxicants, inorganic contaminants cannot be degraded. Therefore, immobilization technique through precipitation and adsorption to solids is a main approach to purify water and soil contaminated by inorganic pollutants.

Montmorillonite, a kind of natural abundant clay mineral, is able to efficiently adsorb heavy metal cations from water through cation exchange of its original cations in the interlayer space.⁵⁻⁸ But it has a very poor affinity for phosphate.⁹ Interestingly, hydroxyl-aluminum (Al_{13}) pillared montmorillonite exhibits a strong affinity for both heavy metal cations and phosphate due to the high reactivity of the surface hydroxyl group.^{8, 10-12} As a low-cost adsorbent, the adsorption capacities of Al_{13} pillared montmorillonites (AIPMTs) toward Cd(II) or phosphate have received a great deal of attention,^{10, 12-14} whereas a simultaneous adsorption of these two contaminants on AIPMTs has received much less attention.

In the environment, however, heavy metal cations and oxyanions often coexist in soil and wastewater, thus their transport and fate may be significantly influenced by each other.¹⁵ For example, the simultaneous adsorption of heavy metal cations and oxyanions on metal (oxyhydr) oxide can decrease

by competition for the adsorption sites, or formation of non-adsorbing cation-oxyanion complex,¹⁶⁻¹⁸ or increase by the formation of ternary surface complexes and surface precipitation.¹⁸⁻²¹ Similar with metal (oxyhydr) oxide containing hydroxyl group, hydroxymetal modified clay minerals might have similar adsorption characteristics with metal (oxyhydr)oxide. Zhu et al.¹⁵ have reported the enhanced co-adsorption of Cd(II) and phosphate on hydroxyiron-montmorillonite complex. As AIPMts have a different structure from hydroxyiron-montmorillonite complex, the simultaneous adsorption of Cd(II) and phosphate on AIPMt is worth studying. According to previous studies, the amount of Al content could affect not only the structure of AIPMt but also the adsorption of Cd(II) or phosphate on AIPMt.^{10, 22, 23} In this work, therefore, the effect of Al/clay ratio on the structure of AIPMt and single/simultaneous adsorptions of Cd(II) or/and phosphate on AIPMts were investigated. Based on the structural characteristics, adsorption and XPS spectra results, the adsorption mechanism of Cd(II) and phosphate on AIPMt was proposed. The results might provide novel information for the adsorption of AIPMt towards heavy metal cations and oxyanions.

2. Materials and methods

2.1 Materials

The calcium montmorillonite (Ca-Mt; purity > 95%) was obtained from Inner Mongolia, China. The cation exchange capacity (CEC) is 110.5 meq/100 g. $\text{AlCl}_3 \cdot 6\text{H}_2\text{O}$, Na_2CO_3 , $\text{Cd}(\text{NO}_3)_2$, and KH_2PO_4 were purchased from Guangzhou Chemical Reagent Factory. All chemicals were analytical grades and used without further purification.

2.2 Preparation of Al_{13} -pillared montmorillonite

A hydroxyl-aluminum solution, containing Al_{13} cations, was prepared by slowly adding a 0.5 M

Na_2CO_3 solution to a 1.0 M solution of AlCl_3 at a rate of 1 mL/min with vigorous stirring in a water bath at 60°C to give a final $\text{OH}^-/\text{Al}^{3+}$ ratio of 2.4. The mixture was continuously stirred for 12 h, after which it was allowed to 'age' for 24 h at 60°C . Montmorillonite was then added to the mixture to give Al/clay ratios of 1.0, 2.0, and 4.0 mmol/g. The dispersion was stirred for 24 h, and then aged for 24 h at 60°C . The product was collected by centrifugation, washed with distilled water, and then freeze-dried for 48 h. Depending on the Al/clay ratio, the Al_{13} -pillared montmorillonites were denoted as AIPMt-1.0, AIPMt-2.0 and AIPMt-4.0, respectively.

2.3 Characterization of adsorbents

Powder X-ray diffraction (XRD) patterns were recorded on a Bruker D8 Advance diffractometer with Ni-filtered $\text{CuK}\alpha$ radiation ($\lambda = 0.154$ nm, 40 kV and 40 mA) with 2.3° Soller slits, 1.0 mm divergence slit and 0.1 mm receiving slit. Patterns were collected between 1° and 20° (2θ) at a scanning speed of 1° (2θ) min^{-1} with a 0.01 2θ step size and a 0.65 s counting time.

Thermogravimetric analysis (TG) was performed on a Netzsch STA 409PC instrument. The samples were heated from 30 to 1000°C at a rate of $10^\circ\text{C}/\text{min}$ under a flow of high-purity nitrogen (60 mL/min).

Nitrogen adsorption-desorption isotherms were determined on samples that had been outgassed under vacuum for 12 h at 120°C , using a Micromeritics ASAP 2020M instrument. The multiple-point Brunauer-Emmett-Teller (BET) method was used to calculate the specific surface area (SSA) of the materials.

X-ray photoelectron spectroscopy (XPS) analyses were carried out on a Thermo Scientific K-Alpha spectrometer equipped with Al $\text{K}\alpha$ source (1486.8 eV). The spectra were collected with pass energy of 30 eV and an analysis area of $400 \mu\text{m}^2$. The C1s peak at 284.8 eV was used as reference to correct the

charging effect. All spectra were performed with Smart background correction. The samples, collected from the adsorption system with 90 mg/L Cd and/or 80 mg/L phosphate, were freeze-dried for 24 h before analysis.

Zeta potentials, determined on Malvern MPT-2/Zetasizer Nano ZS instrument, were used to analyze the isoelectric point. The analysis pH was adjusted using 0.1 M HCl or 0.1 M NaOH solutions. Zeta potentials were determined at least 5 times in each pH setting; the value recorded each time was the average of 15 measurements.

2.4 Adsorption experiments

The adsorption experiments included two different systems: (1) adsorption of a single contaminant; (2) simultaneous adsorption of two contaminants. For system #1, the adsorption of phosphate or Cd(II) was measured with an initial concentration of 20–140 mg/L and 30–240 mg/L for phosphate and Cd(II), respectively. For system #2, adsorption of both phosphate and Cd(II) was investigated simultaneously. The initial concentration of one contaminant was the same as that in system #1 while the concentration of the other was kept constant at 80 mg/L for phosphate or 90 mg/L for Cd(II).

Batch experiments were performed to investigate the adsorption capacities of AIPMTs from aqueous solutions. The initial pH was adjusted to ~ 5.0 (± 0.05) using HCl and KOH. In both systems, 0.1 g of the prepared adsorbents were combined with 20 mL solutions containing different concentrations of phosphate and Cd(II) in a 25 mL glass centrifuge tube with Teflon cover. The tubes were continuously agitated on a shaker for 24 h at 160 rpm and 25°C, and then filtered. The concentration of phosphate in the supernatant was analyzed using the Ascorbic Acid method²⁴ on a UV-Vis spectrophotometer (Perkin Elmer LAMBDA 850) at a wavelength of 880 nm, and that of Cd(II) was determined by atomic absorption spectrometry (Perkin Elmer AAnalyst 400). All the adsorption experiments were, at

least, conducted in duplicate.

3. Results and discussion

3.1 Structure of adsorbents

The thickness of montmorillonite individual layer is 0.96 nm.²⁵ The d_{001} -value for Ca-Mt was 1.48 nm because of the presence of hydrated calcium ions (exchangeable) in the interlayer space (Fig. 1). The basal spacing of AIPMt samples clearly depended on the Al/clay ratios (Fig. 1). The d_{001} -value of 1.89 nm for AIPMt-4.0 corresponded to interlayer separations (distance) of 0.93 nm. This value was close to the size of the Keggin-like $(Al_{13})^{7+}$ cation (0.9 nm), indicating the successful intercalation of Al_{13} into Mt.²⁶ The d_{001} -value of AIPMt-2.0 at 1.88 nm was similar to that of AIPMt-4.0, but the 001 reflection of AIPMt-2.0 was slightly broader than that of AIPMt-4.0, indicating less uniformity of basal spacing in AIPMt-2.0.²⁷ For the AIPMt-1.0, the broad (001) reflection was at the 2θ range of 5–6°, which was between the expansion of the Keggin-containing AIPMt and the d_{001} -value of the parent Ca-Mt. The width of this reflection indicated that variations in the basal spacing occurred.²⁷ Expansion of the interlayer spaces of AIPMt-1.0 by Al_{13} cations occurred some, while expansion of the interlayer spaces were not observed in some.

The TG curves for the samples were depicted in Fig. 2. In the curve for Ca-Mt, two major mass losses were obtained; the mass loss below 200°C was due to the removal of water molecules associated with interparticle and interlayer surfaces while that at 500–700°C was ascribed to layer dehydroxylation. Like that of Ca-Mt, the TG curves for AIPMts showed a large loss of mass below 200°C from the evaporation of adsorbed water, and a mass loss in the range of 200–700°C due to the dehydroxylation of interlayer Al_{13} cations and the layer structure.²⁸⁻³⁰ The mass losses of AIPMts in the temperature

range of 200–500°C mainly corresponded to the dehydroxylation of interlayer Al_{13} cation because of the absence of evidence for mass loss on TG curve of Ca-Mt in this range.²⁹ The mass losses in the range of 200–500°C increased with increase in Al dose from 3.54% for AIPMt-1.0 to 6.33% for AIPMt-4.0 (Table 1), indicating the increase of Al_{13} cation content with increase in Al dose.

Consistent with the results of XRD and TG, the SSA values of AIPMts also increased with increase in Al/clay ratio (Table 1). The SSA values of AIPMts sharply increased from 111.86 m^2/g for AIPMt-1.0 to 254.72 for AIPMt-2.0 m^2/g and 304.94 m^2/g for AIPMt-4.0. The type IV N_2 adsorption-desorption isotherms of AIPMt were indicative of their microporosity (Fig. 3). The steep increase at low relative pressures corresponded to the filling of interpillar micropores in the interlayer space, and the hysteresis loop implied the interparticle mesopores space. With increase in the Al/clay ratio, the adsorbed quantities of N_2 at low relative pressures sharply increased (Fig. 3), indicating increase in micropores after the intercalation of Al_{13} cations.

The zeta potentials of montmorillonite particles were also affected by the intercalation of Al_{13} cation (Fig. 4). The isoelectric point (pH_{zpc}) increased with increase in the loading amount of Al_{13} cations.

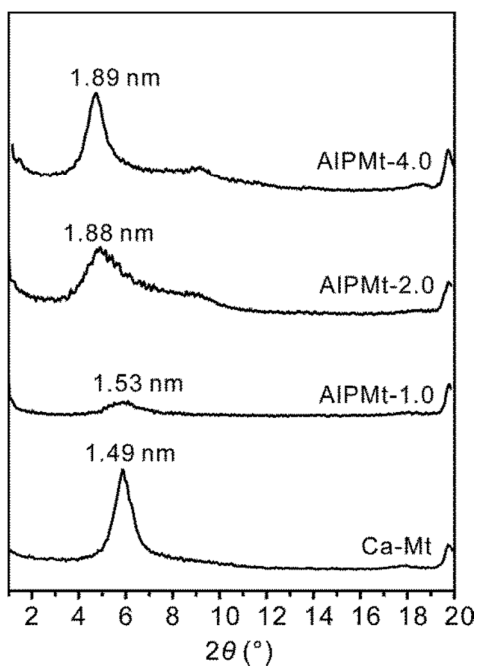


Fig. 1 The X-ray diffraction patterns of raw montmorillonite and Al₁₃ pillared montmorillonites.

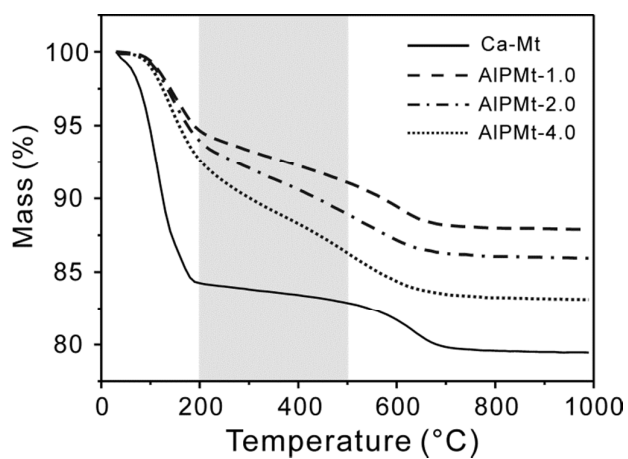


Fig. 2 TG curves of raw montmorillonite and Al₁₃ pillared montmorillonites.

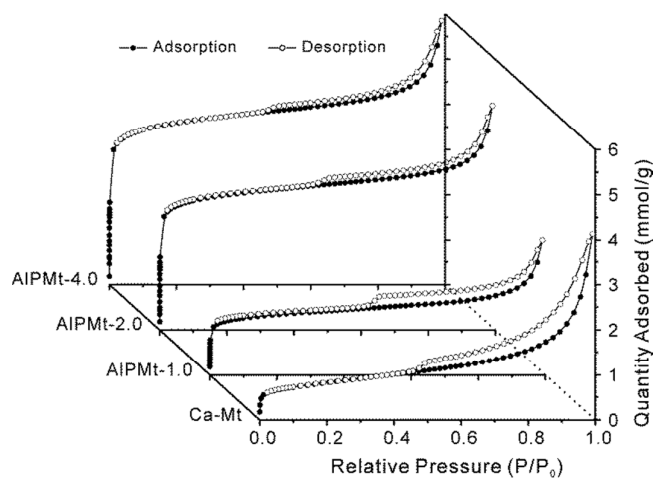


Fig. 3 N_2 adsorption-desorption isotherms of raw montmorillonite and Al_{13} pillared montmorillonites.

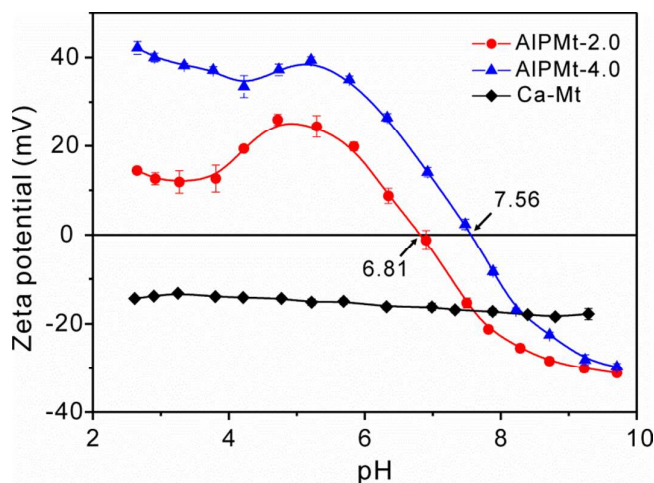


Fig. 4 The zeta potential of raw montmorillonite and Al_{13} pillared montmorillonites.

3.2 Single contaminant adsorption

In the single contaminant adsorption system, the adsorption of phosphate and Cd(II) on AIPMTs significantly depended on the intercalated amount of Al_{13} cations (Fig. 5). The adsorption capacities of AIPMTs towards phosphate increased with increase in intercalated Al_{13} cations (Fig. 5a). On the contrary, for the removal of Cd(II), the adsorption capacities of AIPMTs decreased with increase in intercalated Al_{13} cations (Fig. 5b).

In the case of adsorption of phosphate, the higher adsorption capacities of AIPMTs were attributed to the presence of Al-OH functional group on interlayer Al_{13} cations.^{12, 22, 31-33} Adsorption of phosphate on Al_{13} pillared montmorillonites was mainly controlled by ligand exchange mechanism. The hydroxyl group on Al_{13} cations can be replaced by phosphate, and thus phosphate was adsorbed on the adsorbent while hydroxyl was released to the solution.^{32, 33} The increase in the pH values of the solution after phosphate adsorption was an important evidence for the ligand exchange mechanism (Fig. S1).³²

The adsorption capacities of AIPMTs towards Cd(II) decreased in the order: AIPMt-4.0 < AIPMt-2.0 < AIPMt-1.0 (Fig. 5b). Although AIPMt-4.0 and AIPMt-2.0 had much larger SSA values, their adsorption capacities toward Cd(II) were lower than that of AIPMt-1.0. Montmorillonite is naturally able to efficiently adsorb heavy metal cations from water through cation exchange.⁵⁻⁷ The intercalation of Al_{13} cations, however, resulted in decrease in the adsorption capacities towards Cd(II). Cations with higher charge always have better capability to exchange with the original cation of clay minerals and have stronger electric interaction with the charge sites.³⁴ The high charge of Al_{13} (7+) cations boosted the electric interaction of the charge sites on montmorillonite. As a result, the intercalated Al_{13} cations were not readily exchangeable in the adsorption of Cd(II). According to the XRD and TG result, intercalated Al_{13} cations did not completely occupy the charge sites on AIPMt-1.0 and AIPMt-2.0. Therefore, the exchangeable cations in the interlayer space of AIPMt-1.0 and AIPMt-2.0 were of benefit to the adsorption of Cd(II).

Besides the cation exchange adsorption, Cd(II) could also be adsorbed on the variable charge on the surface of montmorillonites. After treatment with Al_{13} , the pH_{zpc} of AIPMt-2.0 and AIPMt-4.0 increased to 6.81 and 7.56, respectively. When the solution pH (pH 5 in this study) was lower than

their pH_{zpc} , the variable charges on the surface of AIPMt-2.0 and AIPMt-4.0 were positive, which may adversely affect the adsorption of Cd(II).

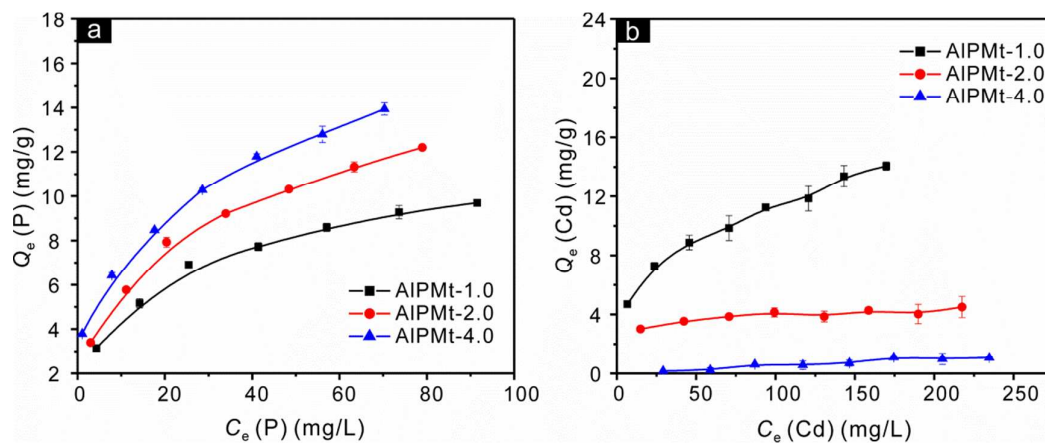


Fig. 5 Adsorption isotherms of phosphate (a) and Cd(II) (b) on AIPMTs in single-solute adsorption system.

3.3 Simultaneous adsorption of phosphate and Cd(II)

According to the adsorption isotherms of phosphate and Cd(II) in simultaneous adsorption system (Fig. 6), more of the contaminants were adsorbed by AIPMTs in the simultaneous adsorption system than in the single adsorption system.

The adsorption quantities of phosphate on all three AIPMTs evidently increased with increase in the initial concentration of Cd(II) (Fig. 6b). When the initial concentration of Cd(II) exceeded 90 mg/L, the adsorption of phosphate gradually reached its maximum (Fig. 6b). Similar to that the observation in the single adsorption system, AIPMt-4.0 with larger amount of Al_{13} cations showed higher adsorption capacity towards phosphate in the simultaneous adsorption system (Fig. 6a,b). With the existence of Cd(II), removals of phosphate by AIPMt-4.0 and AIPMt-2.0 increased by 19.48% and 17.35%, respectively, which were much higher than that by AIPMt-1.0 (3.75%)(Fig. 7a). This

observation implies that the additional adsorption sites for phosphate provided by the adsorption of Cd(II) mainly exist on the surface of Al_{13} cations on AIPMTs.

Similar to the adsorption of phosphate, the adsorptions of Cd(II) on all three AIPMTs were also apparently enhanced in the simultaneous adsorption system (Fig. 6c,d). The removal of Cd(II) on AIPMt-4.0, AIPMt-2.0, and AIPMt-1.0 was enhanced from 3.33%, 21.42%, and 49.28% to 93.31%, 83.83%, and 70.42%, respectively, in the simultaneous adsorption system (Fig. 7b). The adsorption of Cd(II), however, strongly depended on the initial concentration of phosphate and the amount of Al_{13} cations on AIPMTs in the simultaneous adsorption system (Fig. 6c,d). When the initial concentration of phosphate was less than 60 mg/L, the adsorption capacities of AIPMT towards Cd(II) were still in the order: AIPMt-4.0 < AIPMt-2.0 < AIPMt-1.0 (Fig. 6d). But with the increase of initial concentration of phosphate, the adsorption quantities of Cd(II) on AIPMt-4.0 and AIPMt-2.0 were dramatically promoted (Fig. 6d). Then, in a high initial concentration of phosphate (> 60 mg/L) the adsorption capacities of AIPMT towards Cd(II) were in the order: AIPMt-4.0 > AIPMt-2.0 > AIPMt-1.0 (Fig. 6d). These observations indicated that the adsorption of phosphate provided a lot of additional sorption sites for the Cd(II) and the synergistic adsorption sites mainly existed on the surface of Al_{13} cations on AIPMTs.

Compared with the adsorption of phosphate, the adsorption capacity of AIPMt-4.0 towards Cd(II) was more dependent on the initial concentration of phosphate in the simultaneous adsorption system of the present study. Thus, the adsorption sites of Cd(II) on AIPMt-4.0 were mainly provided by the adsorbed phosphate in the simultaneous adsorption system. In the case of AIPMt-1.0, the enhancement of adsorption of Cd(II) was much larger than that of phosphate, indicating that Cd(II) adsorbed by cation exchange might not provide adsorption sites for phosphate. These findings suggested that

Cd(II) was bound to the adsorbed phosphate in the simultaneous adsorption system, with phosphate binding directly to the surface of Al_{13} cations on AIPMTs. The Cd(II) adsorbed by binding to adsorbed phosphate also could in turn provide some additional adsorption sites for phosphate.

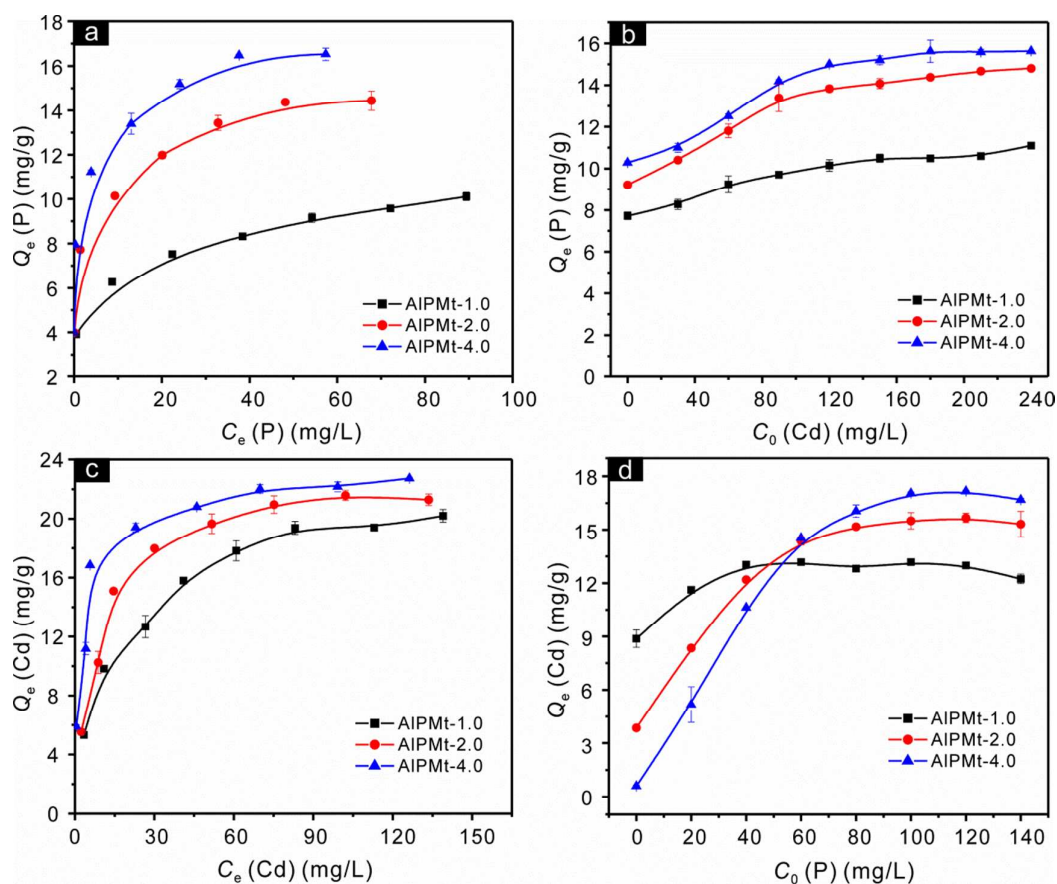


Fig. 6 Simultaneous adsorption results of phosphate and Cd(II) on AIPMTs: (a) adsorption isotherms of phosphate on AIPMTs ($C_{0,Cd} = 90$ mg/L); (b) the effect of initial concentration of Cd(II) on the adsorption quantities of phosphate on AIPMTs ($C_{0,P} = 80$ mg/L); (c) adsorption isotherms of Cd(II) on AIPMTs ($C_{0,P} = 80$ mg/L); (d) the effect of initial concentration of phosphate on the adsorption quantities of Cd(II) on AIPMTs ($C_{0,Cd} = 90$ mg/L).

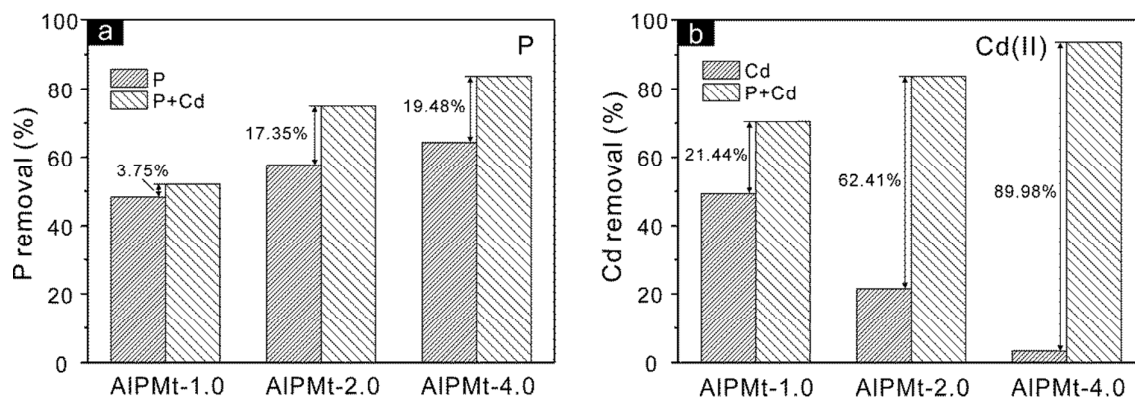


Fig. 7 Comparative adsorption of phosphate (a) and Cd(II) (b) on AIPMts in single (P or Cd) and simultaneous (P + Cd) adsorption system ($C_{0,P} = 80$ mg/L, $C_{0,Cd} = 90$ mg/L).

3.4 Adsorption mechanism

In previous studies, three possible mechanisms have been proposed to account for the synergistic adsorption of metal cations and oxyanions to metal (oxyhydr) oxides, namely: the formation of ternary complexes; surface precipitation; and enhanced electrostatic interaction.^{15, 18, 20, 21, 35, 36}

In the present study, phosphate and Cd(II) might form phosphate-bridge ternary complexes on the surface of Al_{13} cations on AIPMt. That is, the adsorbed phosphate primarily occupied the surface of Al_{13} cations on AIPMt, while most of the adsorbed Cd(II) were attached to the adsorbed phosphate rather than directly to the surface of AIPMt. In order to obtain supporting evidence for this hypothesis, XPS was used to examine the samples after adsorption of contaminants, since XPS has been widely used to assess the interaction of inorganic ions with solid surfaces.

The P2p binding energy of adsorbed phosphate on AIPMt-4.0 in the single adsorption system was slightly higher than that in the simultaneous adsorption system (Fig. 8a). In the single adsorption system, all adsorbed phosphate was bound directly to the surface of AIPMt-4.0 as an inner-sphere complex, giving rise to the large P2p binding energy.¹⁵ In the case of the simultaneous system, a little

part of adsorbed phosphate bound to the adsorbed Cd(II) not directly bound to the surface of AIPMt-4.0, which resulted in the slightly decreased P2p binding energy.¹⁵

As Zhu et al.¹⁵ reported, the Cd3d binding energies of adsorbed Cd directly bound to surface of adsorbent were much larger than that of adsorbed Cd bound to the adsorbed phosphate. Consistent with Zhu et al.,¹⁵ in the present study, Cd3d binding energies, especially Cd3d_{5/2} (406.05 eV) of adsorbed Cd on AIPMt-4.0 in simultaneous-adsorption system were much lower than that in single-adsorption system (Fig. 8b). This finding suggested that the chemical environment of adsorbed Cd in the simultaneous adsorption system was different from that in the single-adsorption system. As such, one would expect that in the simultaneous-adsorption system, the Cd adsorbed was bound to phosphate rather than directly to the surface of AIPMt-4.0.

On the basis of adsorption and XPS results, the strong interaction among intercalated Al₁₃ cations, adsorbed phosphate, and Cd(II) in simultaneous system indicated that the formation of ternary complexes might be primarily responsible for the synergistic adsorption of phosphate and Cd(II) onto AIPMt-4.0. That is, phosphate firstly binds to Al-OH surface of intercalated Al₁₃ cations directly via a ligand-exchange mechanism, forming ≡Al-P inner-sphere complex. Secondly, Cd(II) binds to the adsorbed Phosphate to form ≡Al-P-Cd ternary surface complex. Thirdly, the bound Cd may further adsorb phosphate, forming a ≡Al-P-Cd-P complex. A similar bonding mode was proposed by Zhu et al.¹⁵ for the adsorption of phosphate and Cd(II) on hydroxyiron-montmorillonite complex, and Li et al.¹⁸ for the adsorption of Zn with glyphosate on γ -alumina.

Besides, the contribution of electrostatic attraction for the co-adsorption of phosphate and Cd(II) on AIPMts could not be neglected. The possibility of other applicable adsorption model to the co-adsorption of phosphate and Cd(II) on AIPMt also cannot be ruled out. The models of a ternary

adsorption system might be influenced by solution pH, physiochemical properties of adsorbent, adsorption densities of contaminants.^{15, 18, 20, 21, 35, 36} Therefore, the co-adsorption mechanism of phosphate and Cd(II) on AIPMTs need to be further studied to clarify the binding model.

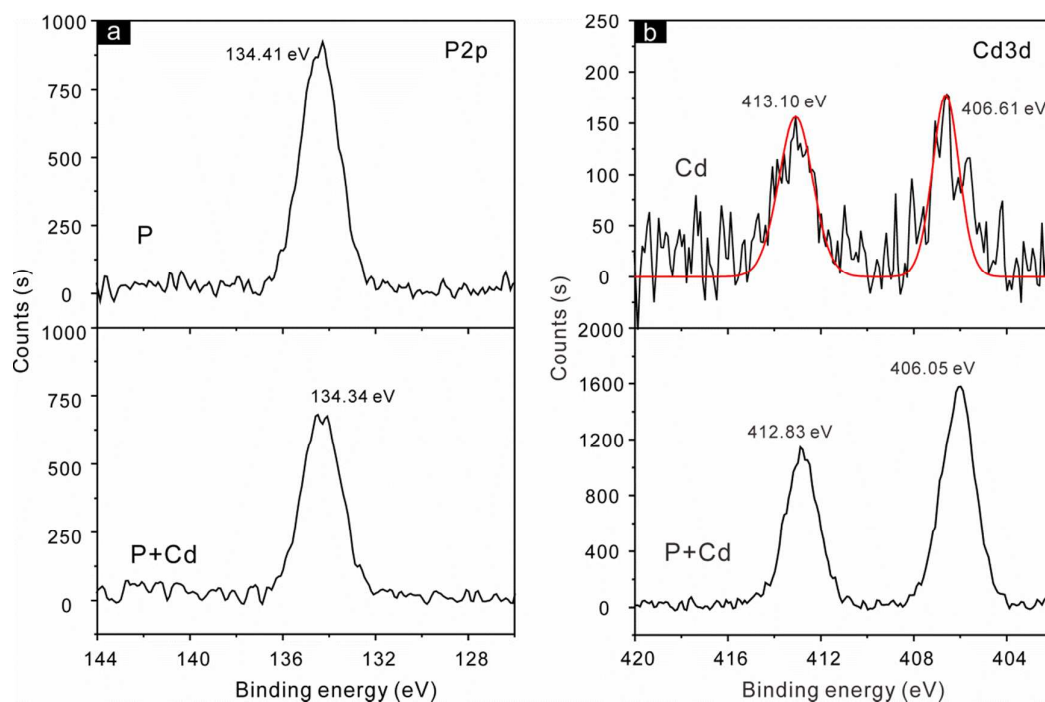


Fig. 8 P2p (a) and Cd3d (b) XPS spectra of AlPMt-4.0 after adsorption in single (P or Cd) and simultaneous (P+Cd) adsorption system.

Conclusions

The adsorption of phosphate and Cd(II) in single and simultaneous adsorption systems was investigated by using Al₁₃ pillared montmorillonite with different Al/clay ratio. The basal spacing, loaded amount of Al₁₃ cations, and the specific surface area of AIPMTs increased with increase in Al/clay ratio. With increase in the loaded amount of Al₁₃ cations, the adsorption capacities of AIPMTs toward phosphate increased, but that toward Cd(II) dramatically decreased in the single-adsorption

system. In the simultaneous-adsorption system, however, the adsorption of both phosphate and Cd(II) on AIPMts increased with the increase of loaded amount of Al₁₃ cations, so did the enhancement of adsorption capacities of AIPMts toward both contaminants. The adsorption capacities of AIPMts with higher loaded amount of Al₁₃ cations toward Cd(II) were significantly promoted in the simultaneous-adsorption system, indicating that the surface of intercalated Al₁₃ cations were the co-adsorption sites. Combined with XPS spectra, the formation of phosphate-bridged ternary surface complexes might be primarily responsible for the co-adsorption of phosphate and Cd(II) onto AIPMt-4.0. Hence, the AIPMts could efficiently remove both phosphate and Cd(II) from water, and might be a novel adsorbent for sequestration of heavy metal cations and oxyanions.

Acknowledgments

We gratefully acknowledge the financial support from the National Natural Science Foundation of China (Grant No. 41322014, 41272060, U1201233), Guangdong Provincial Program for Support of Top-notch Young Professions (Grant No. 2014TQ01Z249), the CAS-SAFEIA International Partnership Program for Creative Research Team (Grant No. 20140491534), and Youth Innovation Promotion Association CAS (Grant No. 2014324). Dr Xi thanks the Queensland University of Technology's Vice Chancellor's research grant. We specially acknowledge Dr Hongmei Liu from Guangzhou Institute of Geochemistry, Chinese Academy of Sciences (GIGCAS) for help with XPS analyses. The first author also thanks China Scholarship Council (CSC) for financial support. This is contribution No. IS-2128 from GIGCAS.

References

1. D. L. Sparks, *Elements*, 2005, **1**, 193-197.
2. USEPA, *TSCA work plan for chemical assessments: 2014 update*, U.S. Environment Protection Agency (Ed.), 2014.
3. B. Pernet-Coudrier, W. X. Qi, H. J. Liu, B. Muller and M. Berg, *Environ. Sci. Technol.*, 2012, **46**, 5294-5301.
4. W. Li, X. H. Feng, Y. P. Yan, D. L. Sparks and B. L. Phillips, *Environ. Sci. Technol.*, 2013, **47**, 8308-8315.
5. T. Undabeytia, S. Nir, G. Rytwo, E. Morillo and C. Maqueda, *Clay Clay Miner.*, 1998, **46**, 423-428.
6. T. Undabeytia, S. Nir, G. Rytwo, C. Serban, E. Morillo and C. Maqueda, *Environ. Sci. Technol.*, 2002, **36**, 2677-2683.
7. E. Alvarez-Ayuso and A. Garcia-Sanchez, *Clay Clay Miner.*, 2003, **51**, 475-480.
8. G. D. Yuan, B. K. G. Theng, G. J. Churchman and W. P. Gates, in *Developments in Clay Science*, eds. F. Bergaya and G. Lagaly, Elsevier, 2013, vol. 5B, ch. 5.1, pp. 587-644.
9. L. Borgnino, C. E. Giacomelli, M. J. Avena and C. P. De Pauli, *Colloid Surface A*, 2010, **353**, 238-244.
10. L. G. Yan, X. Q. Shan, B. Wen and G. Owens, *J Hazard Mater*, 2008, **156**, 499-508.
11. P. X. Wu, W. M. Wu, S. Z. Li, N. Xing, N. W. Zhu, P. Li, J. H. Wu, C. Yang and Z. Dang, *J. Hazard. Mater.*, 2009, **169**, 824-830.
12. L. G. Yan, Y. Y. Xu, H. Q. Yu, X. D. Xin, Q. Wei and B. Du, *J. Hazard. Mater.*, 2010, **179**, 244-250.
13. D. Karamanis and P. A. Assimakopoulos, *Water Res.*, 2007, **41**, 1897-1906.

14. M. L. Schlegel and A. Manceau, *Environ. Sci. Technol.*, 2007, **41**, 1942-1948.
15. R. L. Zhu, M. Li, F. Ge, Y. Xu, J. X. Zhu and H. P. He, *Clay Clay Miner.*, 2014, **62**, 79-88.
16. M. M. Benjamin and J. O. Leckle, *Environ. Sci. Technol.*, 1982, **16**, 162-170.
17. T. L. Theis and M. J. West, *Environ. Technol. Lett.*, 1986, **7**, 309-318.
18. W. Li, Y. J. Wang, M. Q. Zhu, T. T. Fan, D. M. Zhou, B. L. Phillips and D. L. Sparks, *Environ. Sci. Technol.*, 2013, **47**, 4211-4219.
19. C. Maqueda, E. Morillo and T. Undabeytia, *Soil Sci.*, 2002, **167**, 659-665.
20. P. J. Swedlund, J. G. Webster and G. M. Miskelly, *Geochim. Cosmochim. Acta*, 2009, **73**, 1548-1562.
21. E. J. Elzinga and R. Kretzschmar, *Geochim. Cosmochim. Acta*, 2013, **117**, 53-64.
22. L. Z. Zhu and R. L. Zhu, *Sep. Purif. Technol.*, 2007, **54**, 71-76.
23. M. X. Zhu, K. Y. Ding, S. H. Xu and X. Jiang, *J. Hazard. Mater.*, 2009, **165**, 645-651.
24. USEPA, *Method 365.2, Methods for chemical analysis of water and wastes*, U.S. Environmental Protection Agency (Ed.), 2nd Edition, Washington, DC., 1983.
25. F. Bergaya and G. Lagaly, in *Developments in Clay Science*, eds. F. Bergaya and G. Lagaly, Elsevier, 2013, vol. 5A, ch. 1, pp. 1-19.
26. D. Plee, F. Borg, L. Gatinéau and J. J. Fripiat, *J. Am. Chem. Soc.*, 1985, **107**, 2362-2369.
27. S. M. Thomas and M. L. Occelli, *Clay Clay Miner.*, 2000, **48**, 304-308.
28. J. T. Kloprogge and R. L. Frost, *Appl. Clay Sci.*, 1999, **15**, 431-445.
29. M. L. Occelli, A. Auroux and G. J. Ray, *Microporous Mesoporous Mater.*, 2000, **39**, 43-56.
30. L. Y. Ma, J. X. Zhu, H. P. He, Y. F. Xi, R. L. Zhu, Q. Tao and D. Liu, *Appl. Clay Sci.*, 2015, **112-113**, 62-67.

31. U. K. Saha, S. Hiradate and K. Inoue, *Soil Sci. Soc. Am. J.*, 1998, **62**, 922-929.
32. T. Kasama, Y. Watanabe, H. Yamada and T. Murakami, *Appl. Clay Sci.*, 2004, **25**, 167-177.
33. R. L. Zhu, L. Z. Zhu, J. X. Zhu, F. Ge and T. Wang, *J. Hazard. Mater.*, 2009, **168**, 1590-1594.
34. R. L. Zhu, T. Wang, F. Ge, W. X. Chen and Z. M. You, *J. Colloid Interface Sci.*, 2009, **335**, 77-83.
35. C. R. Collins, K. V. Ragnarsdottir and D. M. Sherman, *Geochim. Cosmochim. Acta*, 1999, **63**, 2989-3002.
36. M. Grafe, M. Nachtegaal and D. L. Sparks, *Environ. Sci. Technol.*, 2004, **38**, 6561-6570.

Figure captions:

Fig. 1 The X-ray diffraction patterns of raw montmorillonite and Al₁₃ pillared montmorillonites.

Fig. 2 TG curves of raw montmorillonite and Al₁₃ pillared montmorillonites.

Fig. 3 N₂ adsorption-desorption isotherms of raw montmorillonite and Al₁₃ pillared montmorillonites.

Fig. 4 The zeta potential of raw montmorillonite and Al₁₃ pillared montmorillonites.

Fig. 5 Adsorption isotherms of phosphate (a) and Cd(II) (b) on AIPMts in single-solute adsorption system.

Fig. 6 Simultaneous adsorption results of phosphate and Cd(II) on AIPMts: (a) adsorption isotherms of phosphate on AIPMts ($C_{0,Cd} = 90$ mg/L); (b) the effect of initial concentration of Cd(II) on the adsorption quantities of phosphate on AIPMts ($C_{0,P} = 80$ mg/L); (c) adsorption isotherms of Cd(II) on AIPMts ($C_{0,P} = 80$ mg/L); (d) the effect of initial concentration of phosphate on the adsorption quantities of Cd(II) on AIPMts ($C_{0,Cd} = 90$ mg/L).

Fig. 7 Comparative adsorption of phosphate (a) and Cd(II) (b) on AIPMts in single (P or Cd) and simultaneous (P + Cd) adsorption system ($C_{0,P} = 80$ mg/L, $C_{0,Cd} = 90$ mg/L).

Fig. 8 P2p (a) and Cd3d (b) XPS spectra of AIPMt-4.0 after adsorption in single (P or Cd) and simultaneous (P+Cd) adsorption system.

Table 1 Characterization results of original montmorillonite and Al₁₃ pillared montmorillonites.

Samples	d_{001} (nm)	Mass loss (200–500 °C, wt.%)	Specific surface area (m ² /g)
Ca-Mt	1.49	1.93	65.64
AlPMt-1.0	1.53	3.54	111.86
AlPMt-2.0	1.88	5.01	254.72
AlPMt-4.0	1.89	6.33	304.94